Noname manuscript No.
(will be inserted by the editor)

Computational multicellular systems biology in cancer:

Simulating the impact of parenchymal fluid flow and tissue mechanics on colon cancer metastases of the liver⋆

Paul Macklin[∗,†] **· Jessica Sparks**[†] **·**
Hermann B. Frieboes · Erik Brodin ·
Ahmadreza Ghaffarizadeh · Shannon M. Mumenthaler

Dedicated to all the papers we should have written.

the date of receipt and acceptance should be inserted later

Abstract 150-250 words This is an awesome paper!

Keywords Neat · Cool

Mathematics Subject Classification (2000) MSC codes

PACS PACS codes

CR Subject Classification CR codes

⋆ Better titles appreciated

∗ Invited and corresponding author

† Contributed equally to this work

P. Macklin · A. Ghaffarizadeh · S.M. Mumenthaler
Lawrence J. Ellison Institute for Transformative Medicine, University of Southern California, 2250 Alcazar St., CSC-248, Los Angeles, CA 90033, USA
Tel.: 310-701-5785, E-mail: Paul.Macklin@MathCancer.org, www: `http://MathCancer.org`
H.B. Frieboes
DEPARTMENT, University of Louisville, ADDRESS, Louisville, KY ZIP, USA

J. Sparks · E. Brodin
Dept. of Chemical, Paper and Biomedical Engineering, Miami Univiersity, (address), Oxford, OH ZIP, USA

Fig. 1 Overall schematic of trading insights between models.

1 Introduction

Paul, Jessica, and Shannon write. Different models give different insights. We are working to integrate these insights. Continuum model helps motivate discrete model. Discrete model helps motivate continuum model. Part of a larger-scale effort to dynamically link codes, create open source framework for experimentally-driven multicellualr systems biology. Paul

1. Colon cancer metastasizes to the liver. big clinical problem. bad. Jessica, Shannon
2. Impact of TME unknown, but does impact prognosis Jessica, Shannon
3. Impact of parenchymal mechanics and flow on growth poorly understood, as is the biology regulating tumor-parenchyme interactions at the tumor boundary. Jessica, Shannon
4. New emerging platforms allow you to directly problem some dynamics, but can't measure everything. Difficult ot measure flow dynamics at small scales, in and aroudn foci. Modeling can help. Jessica, Shannon
5. open questions:
   (a) Where do mets most commonly seed? Jessica, Shannon
   (b) How do they alter mechanics adn flow of the liver? Jessica, Hermann
   (c) How do cancer cells impact surrounding hepatocytes? Jessica, Shannon
   (d) Tumor cells are often densely packed, but lower cell-cell adhesion? So, is relative permeability higher or lower? Impact on growth dynamics? Jessica, Paul, Hermann
6. math modeling is a way to fill in the missing pieces, generate testable hypotheses. Paul, Jessica, Hermann
7. Give flavor of past modeling results. Note that most is tissue regeneration, toxicology, or single-scale models of flow. Paul, Jessica, Hermann
8. And now the fun twist: in most multiscale investigations, discrete or smaller-scale simulations are used to generate insights for larger-scale continuum models. Here, we do the opposite: use a very detailed continuum model of flow, mechanics to generate insights to build a discrete multicellular model. Paul

1.1 Background biology Shannon

Describe backround biology of liver (structurally: lobules with outflow from portal triads through parenchyma (sinusoids – cords of heaptocytes surrounding channels, or sinusoids that are lined by thin, fenestratedendothelial cells), flowing out through central veins). Main role: metabolize toxins, act as a giant reactive blood sponge. :-) Also creates bile, but not main focus here. See Fig. 2.

Anything else on the environment. General mechanics? General oxygenation?

Then, the background of colon cancer mets. A preferred site for colon cancer metastases. Properties of most incomign cells. Things like this.

Anything that Shannon things belongs here!

Figure: overall liver geometry.

Fig. 2 Main organization of liver tissue

1.2 Prior modeling works Jessica, Paul,Hermann

Describe past modeling efforts, limite insights, still not enough for CRC mets. Prior modeling restricted to colon cancer mets in liver, and potentially relevant liver models (most of which are focused on tissue engineering, healing, toxicology) Paul, Jessica,Hermann

Short literature review on prior models of liver flow, mechanics. Note much focused on PKPD, toxicity, strong work by Glazier group. Note much work on regeneration, strong work by Drasdo group. Others on flow. Little integration of these works. Pull from our NSF proposal. Paul, Jessica,Hermann

1.3 Overall approach Paul

We willl investigate using two modeling approaches. First, in Section 2 we will use the PVE model to udnerstand flow, mechanics across a typical lobule, and to generate more insights on the fluid / mechanical state of the liver environment surrounding small tumor foci.

In Section 3, we will use agent-based model to investigate cell and tisue biomechanics, transport-limited growth, and tumor-parenchymal interactions on growing tumor foci. Work will direclty incorporate insights from PVE.

2 First approach: Poroviscoelastic (PVE) model Jessica

Short intro. 1 paragraph at most.

2.1 Method

2.2 Results

3 Second approach: Agent-based (PhysiCell) model Paul,Hermann

Short intro. 1 pararaph at most. Note difficulty of adding interstitial flow at this scale. Kasia Rejnia did it with IBcell, but very small domains. Hermann did it in continuum tumor growth model. Jessica did it above in static tumor models. We're doing first-of-its-kind 1 cm2 simulations, hundreds of lobules. So, we use insights from above to come up wtih good approximation.

3.1 Method

Describe the model of several liver lobules. Include overall geometry, overall approach:

1. Model flow as quasi-steady, due to fast time scale
2. Approximate flow as radially symmetric profile in each liver lobules, and extrapolate out to liver boundaries
3. Assume biotransport is

   blah

3.1.1 Generating large 2-D liver tissues

To generate a large liver tissue, we (1) randomly place central veins (CVs) across the tissue, with mean density $\sim 2\times10^{-6}\mu\text{m}^{-2}$ (to ensure a mean hepatic lobular diameter of 800 μm); (2) replace any closely-spaced pairs of CVs with a single CV placed at their midpoint; and (3) we fill the remaining space with parenchymal agents. As needed, we can estimate the lobular boundaries by generating a Voronoi mesh from the central vein positions, and place portal triads at the corners of the mesh. In this paper, we generated a 1 cm^2 liver tissue containing 233 hepatic lobules. See Fig. 3

We have included a MATLAB script in the supplementary materials to implement this algorithm. It has the random seed hard-coded to reproduce the liver tissue used in this manuscript.

3.1.2 Integrating PVE insights: biotransport in unobstructed liver tissue

We model biotransport in the liver tissue based upon the insights gained from the PVE model; see Section **??**. In regions not occupied by tumor tissue, we assume that hepatic blood and interstitial flow are intact. (Hereafter, we refer to hepatic blood and interstitial flow collectively as "flow" for simplicity.) Moreover, we can assume that on the time scale of tissue mechanics (minutes to hours) and tumor cell proliferation (hours, days, and weeks), that flow occurs on a much faster time scale (seconds), and so biotransport is at quasi-steady state. Moreover, we will approximate flow as radially-symmetric in lobules not obstructed by tumor. Thus, we approximate $\mathbf{u} = -u(r)\hat{\mathbf{r}}$, where $\hat{\mathbf{r}}$ is the radial

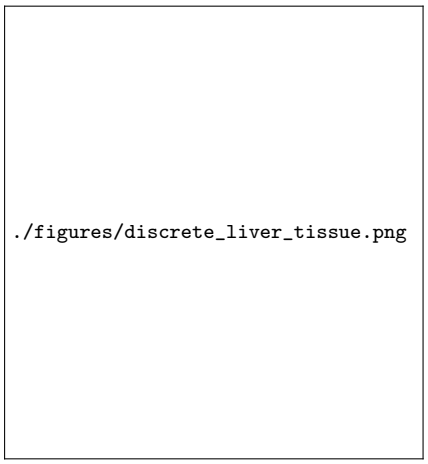

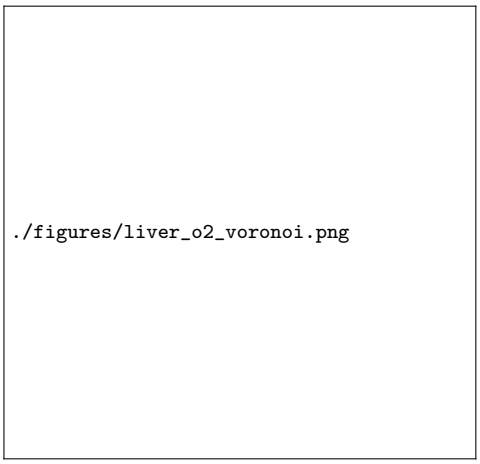

Fig. 3 Left: 1 cm^2 generated slice of liver tissue. Open sections are central veins, and red points are portal triads. **Right:** Oxygenation profile using the "unobstructed liver" approximation in Section 3.1.3. Central veins are superimposed as green points, and used to generate lobular boundaries (red lines) as a Voronoi mesh. Portal triads (left plot) are placed at the corners of the Voronoi mesh.

unit vector (oriented outward from the nearest central vein), and $u(r)$ is the non-negative radial speed profile.

We model the transport of a single growth substrate σ (e.g., oxygen or glucose) in the tissue with

$$\frac{\partial \sigma}{\partial t} = -\nabla \cdot \mathbf{J} - \lambda \sigma \tag{1}$$

$$\mathbf{J} = -D\nabla\sigma + \sigma\mathbf{u}, \tag{2}$$

where $\mathbf{J}$ is the growth substrate flux, λ is its consumption rate, and D is its diffusion coefficient, which we assume is constant.

To understand the relative contribution of the diffusional term in unobstructed flow, we nondimensionalize space with scale L, time with scale $\bar{t}$, and the flow with typical magnitude $\bar{u}$. With these scales, Equations 1-2 become

$$\frac{\partial \sigma}{\partial t} = \left(\frac{D\bar{t}}{L^2}\right)\nabla^2\sigma - \left(\frac{\bar{u}\bar{t}}{L}\right)\nabla\cdot(\sigma\mathbf{u}) - (\lambda\bar{t})\,\sigma. \tag{3}$$

Choosing

$$\frac{u\bar{t}}{L} = 1 \text{ and } \lambda\bar{t} = 1 \Longrightarrow \bar{t} = \frac{1}{\lambda} \text{ and } L = \frac{u}{\lambda}, \tag{4}$$

then the nondimensionalized equation becomes

$$\frac{\partial \sigma}{\partial t} = \left(\frac{D\lambda}{\bar{u}^2}\right)\nabla^2\sigma - \nabla\cdot(\sigma\mathbf{u}) - \sigma. \tag{5}$$

By (Ghaffarizadeh et al. 2016), $D \sim 10^5 \mu\text{m}^2/\text{min}$ and $\lambda \sim 10\ \text{min}^{-1}$. By the PVE work in Section **??** and Nishii et al. (2016), $\bar{u} \sim 10^{-4}\text{m/sec} \sim 10^4\ \mu\text{m/min}$. The diffusion term has relative order of magnitude

$$\frac{D\lambda}{\bar{u}^2} \sim 10^{-2}. \tag{6}$$

Thus, in unobstructed regions of liver lobule, flow is primarily advective-reactive, and we can simplify the original equation to

$$\frac{\partial \sigma}{\partial t} = -\nabla \cdot (\sigma \mathbf{u}) - \lambda \sigma. \tag{7}$$

Next, assuming incompressible flow ($\nabla \cdot \mathbf{u} = 0$) and that $\mathbf{u} \approx -u(r)\hat{\mathbf{r}}$, we have

$$\frac{\partial \sigma}{\partial t} = u(r) \nabla \sigma \cdot \hat{\mathbf{r}} - \lambda \sigma \tag{8}$$

$$= u(r) \frac{\partial \sigma}{\partial r} - \lambda \sigma. \tag{9}$$

Under quasi-steady conditions, $\sigma = \sigma(r)$, and we have

$$0 = \sigma'(r) - \frac{\lambda}{u(r)} \sigma, \Longrightarrow \tag{10}$$

whose analytical solution is given by

$$\sigma(r) = c e^{\lambda \int_0^r \frac{1}{u(s)} ds} \tag{11}$$

for some constant c.

For simplicity, we will approximate the flow profiles in Section **??** with the form

$$u(r) \approx a e^{-br} \tag{12}$$

for constants a and b. Notice that $u(0) = a$ and $u(R) = ae^{-bR} = u(0)e^{-bR}$, whereby

$$b = -\frac{\ln\left(\frac{u(R)}{u(0)}\right)}{R}. \tag{13}$$

For consistency with the PVE model, we set $R = 400\ \mu\text{m}$.

For this simplified form, we have

$$\sigma(r) \approx c e^{\frac{\lambda}{ab}\left(e^{br} - 1\right)}. \tag{14}$$

In Section **??**, we see that $\frac{u(R)}{u(0)}$ is on the order of 0.01 to 0.1, so we choose 0.05. Thus, $b \sim 0.0075\ \mu\text{m}^{-1}$ by Equation 13. Moreover, $u(0) = a \sim 10^{-3}\,\text{m/sec} = 6 \times 10^4\,\mu\text{m/min}$. Tsukada and Suematsu (2012) report that liver oxygenation is approximately 38.9 mmHg in central venules, 48.2 mmHg in sinusoids, and 59.8 mmHg in portal venules. So, we set $\sigma(0) = 38.9$ mmHg:

$$u(r) = 6 \times 10^4 e^{-0.0075r} \tag{15}$$

$$\sigma(r) = 38.9 e^{0.0223\left(e^{0.0075r} - 1\right)}. \tag{16}$$

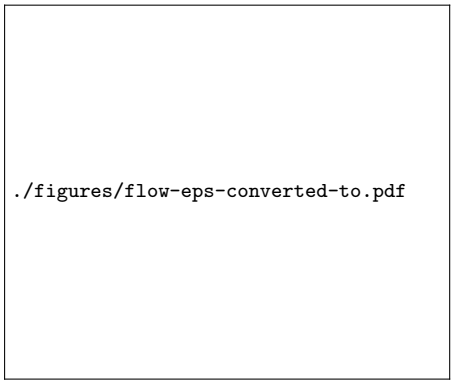

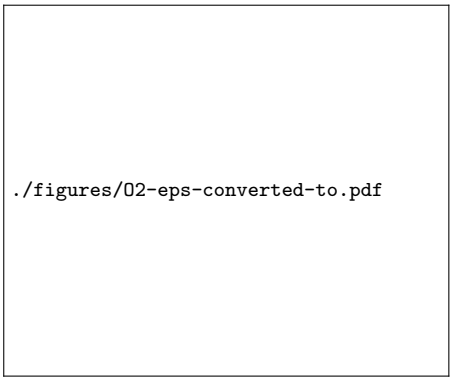

Fig. 4 Sample flow profile (left) and oxygenation profile (right) in a hepatic lobule, under the flow assumptions derived from the PVE model.

We plot the radial flow and oxygenation profiles for these parameters in a hepatic lobule with radius $R = 400\,\mu$m in Fig. 4; note that $\sigma(R) \approx 60$ mmHg, comparable to the portal venule oxygenation reported in Tsukada and Suematsu (2012).

3.1.3 Approximating oxygen transport in large unobstructed liver tissues

As described in Section 3.1.1, we generated a large 1 cm^2 section of liver tissue with many hepatic lobules. Let $\{\mathbf{x}_i\}_{i=1}^n$ denote the centers of the hepatic lobules. We use the analytical solution from Section 3.1.2 to approximate the quasi-steady oxygenation pO_2 in regions of intact, adevective flow-dominated tissue. If

$$r(\mathbf{x}) = \min\left\{||\mathbf{x}_i - \mathbf{x}||\right\}_{i=1}^n \tag{17}$$

is the distance between $\mathbf{x}$ and the nearest central vein, then we approximate

$$\mathrm{pO}_2(\mathbf{x}) = \sigma\left(r(\mathbf{x})\right). \tag{18}$$

Here, σ is the radial oxygenation profile defined in Equation 16.

Note that this is equivalent to partitioning the 2-D tissue cross-section into a Voronoi mesh (with portal triads at the vertices (representing the flow source) and central veins in the centers) and assuming radial flow within each Voronoi polygon. See Fig. 3.

3.1.4 Integrating PVE insights: biotransport within tumors

In Section **??**, we saw that regardless of the relative (fluid) permeability of tumor tissue compared to normal liver parenchymal tissue, tumors with high interstitial fluid pressure (IFP) experience a near complete collapse of flow. High IFP is frequently reported in the literature for solid tumors, particularly

Parameter	Biophysical meaning	Value	Reference
R	cell radius		
R_{N}	nuclear radius		
f_{F}	cell fluid fraction	0.75	
$\bar{b}$	reference cell birth rate		
σ_N	threshold oxygen value for necrosis	5 mmHg	
T_A	mean duration of apoptosis	8.6 hours	
R_{A}	maximum cell adhesion distance	1.5 R	
C_{cca}	cell-cell adhesion parameter		
C_{ccr}	cell-cell repulsion parameter		
$\vdots$			

Table 1 Tumor cell parameters, using PhysiCell Version 1.0.0.

larger ones with necrotic cores (**?**). For simplicity, we shall assume that IFP is sufficiently high in all tumor tissue to disrupt flow, switching biotransport from advective-reactive to diffusive-reactive. Thus, in tumor tissue, we model

$$\frac{\partial \sigma}{\partial t} = D\nabla^T \sigma - \lambda\sigma, \tag{19}$$

where $D = 10^5 \mu\mathrm{m}^2/\mathrm{min}$ and $\lambda = 10\ \mathrm{min}^{-1}$ as in Ghaffarizadeh et al. (2016).

as time permits: In Section **??**, we examine the impact of relaxing this assumption, by assuming that IFP increases with distance from the nearest parenchymal agent, and that flow is eliminated (and hence biotransport is diffusive-reactive) beyond a fixed distance L_{cutoff} from functional parenchyme. May need an additional necrosis mechanism

3.1.5 Tumor cell agents

We model tumor cells using PhysiCell Version 1.0.0 (Ghaffarizadeh et al. 2016 (in review). We use the built-in "live" cell cycle model, with the default models of apoptosis and necrosis. Thus, each cell agent can be Live, Apoptotic, or Necrotic. Apoptosis is modeled as TME-independent, with a constant apoptotic death rate d_A and a stochastic duration with mean T_A. We model necrosis as oxygen-dependent: cells enter the necrotic state if $\sigma < \sigma_N$, and then progress as described in Ghaffarizadeh et al. (2016 (in review). The rate of cell birth depends upon oxygenation as:

$$b(\sigma) = \bar{b}\left(\frac{\sigma - \sigma_N}{\bar{\sigma} - \sigma_N}\right) \tag{20}$$

for reference values $\bar{b}$ and $\bar{\sigma}$.

Tumor cells adhere to tumor and parenchymal agents, and push back with a "repulsive" restorative force as described in Ghaffarizadeh et al. (2016 (in review). We do not consider the impact of cell motility in this paper. Parameter values are given in Table 1.

3.1.6 Parenchymal agents

Rather than model the individual hepatocytes and endothelial cells down to the sinusoidal microarchitectural scale, we model the overall parenchymal tissue as a collection of parenchymal agents, using the "live" cell cycle model, with the apoptotic death model (with stochastic duration). We assume that in the abscence of tumor cells, the tissue is in homeostasis with the birth rate and death rate both set to zero.

also cite Luigi's work
`https://hal.archives-ouvertes.fr/hal-00361051/file/final.pdf`

The parenchymal agents exhange adhesive and "repulsive" forces with other parenchymal agents and tumor cells using the default mechanics model in PhysiCell. In addition, we extend our plasto-elastic model from D'Antonio et al. (2013) to model parenchymal tissue deformation. To model elasticity, we assign each parenchymal agent i (with position $\mathbf{x}_i$) a "reference" point $\mathbf{x}_{i,\mathrm{R}}$, and define the deformation $\mathbf{d}_i(t)$ by

$$\mathbf{d}_i(t) = \mathbf{x}_{i,\mathrm{R}}(t) - \mathbf{x}_i(t). \tag{21}$$

Where needed, define $d_i(t) = ||\mathbf{d}_i(t)||$.

After evolving the agent's position with the built-in PhysiCell mechanics model (see Ghaffarizadeh et al. (2016 (in review)), we further update the agent's position based upon the tissue elasticity:

$$\frac{d}{dt}\mathbf{x}_i = r_{\mathrm{E}}\mathbf{d}_i. \tag{22}$$

To model plastic reorganization of the parenchymal tissue, we evolve $\mathbf{x}_{i,\mathrm{R}}$:

$$\frac{d}{dt}\mathbf{x}_{i,\mathrm{R}} = -r_{\mathrm{P}}\mathbf{d}_i \tag{23}$$

3.1.7 Integrating PVE insights: Constitutive relations for apoptosis

In Section **??**, we saw that there are significant fluid sheers and stress forces at the tumor-parenchymal interface. Such stresses are known to induce apoptosis (**?**). Thus, we will examine theree alternative constitutive relations for apoptosis of the parenchymal cells.

Apoptosis model 1: contact-based apoptosis (AM1) If a parenchymal agent i is in contact with a tumor cell, we set its state to apoptotic.

Apoptosis model 2: deformation-based apoptosis (AM2) If a parenchymal agent i has $d_i(t) > d_{\max}$, we set its state to apoptotic.

Apoptosis model 3: accumulated deformation-based apoptosis (AM3) If a parenchymal agent i has $\int_0^t d_i(s)\,ds > D_{\max}$, we set its state to apoptotic.

3.1.8 Numerical methods

We implemented the model in PhysiCell Version 1.0.0 (Ghaffarizadeh et al. 2016 (in review), with BioFVM Version 1.1.14 (Ghaffarizadeh et al. 2016) to solve the oxygen biotransport equation. In regions of intact flow, we use "Dirichlet nodes" to impose the approximated oxygenation profile from Section 3.1.3. We retain the PhysiCell time step sizes: $\Delta t_{\text{diffusion}} = 0.01$ min, $\Delta t_{\text{mech}} = 0.1$ min, and $\Delta t_{\text{cell}} = 6$ min. (We could solve to quasi-steady state once every 3 hours, but I'd worry about mechanics in that instance.) Each simulation investigated 30 days of tumor growth.

‘

3.1.9 Agents

Describe tumor cell agents: substrate-driven growth, apoptosis, necrosis. Cell-cell adhesion, repulsion. Assume no motiltiy for now. Proliferation rate:

$$a \tag{24}$$

Apoptosis rate

$$a \tag{25}$$

Necrosis rate

$$a \tag{26}$$

Describe parenchyma agents. Rather than model individual hepatocytes, endothelial cells, model parenchyma as a collection of agents, diameter 30 μm. Each parenchyma agent will follow regular adhesion-repulsion mechanics. In addition, we model mechanica interactions with underlying ECM. Each agent i is attached to ECM at $\mathbf{x}_{i,\text{ECM}}$, and experiences an elastic force. Let $\mathbf{d}_i = \mathbf{x}_{i,\text{ECM}} - \mathbf{x}_i$, and let $d_i = ||\mathbf{d}_i|| - R_i$ denote the ellastic deformation. Then we use a force of the form

$$\frac{d}{dt}\mathbf{x}_i(t) = r_{\text{ECM}} d_i \frac{\mathbf{d}_i}{||\mathbf{d}_i||} \tag{27}$$

To model plastic reorganization, we will evolve $\mathbf{x}_{i,\text{ECM}}$ by

$$\frac{d}{dt}\mathbf{x}_{i,\text{ECM}} = r_{\text{mech}} \left(\mathbf{x}_i - \mathbf{x}_{i,\text{ECM}}\right) \tag{28}$$

We shall not model proliferation in the parenchyma, instead assuming that it begins in a state of homeostasis. However, each agent (representnig a small section of tissue), will ahve a probabiltiy of apoptosing. IN this paper, we will investigate the following sub-models

Model 1: Parenchymal agents enter apoptotic state if

Model 2: Parenchymal agents enter apoptotic state if deformation d_i exceeds a threshold

Model 3: Parenchymal agents enter apoptotic state if cumulative deformation $\int_0^t d_i(s)\, ds$ exceeds a threshold.

3.1.10 Integrating insights from the PVE model: mechanics

3.1.11 Parameter estimation

3.1.12 Numerical solution method

Here’s where we say it’s implemented in BioFVM Version (?) for PDE solvers, and PhysiCell Version (?) for agent-based model.

3.2 Results

3.2.1 Model results: dynamics for small tumor foci, no parenchyme apoptosis

Use the assumptions from small tumors. (Good flow in tumors, so no diffusion, no gradients, parenchyme cells moved).

3.2.2 Model results: dynamics for small tumor foci, delayed parenchyme apoptosis

Use the assumptions from small tumors. (Good flow in tumors, so no diffusion, no gradients, parenchyme cells moved, assume the apoptose if moved too far).

3.2.3 Model results: dynamics for larger tumor foci, delayed parenchyme apoptosis

Use the assumptions from larger tumors. (Poor flow in tumors, diffusion, parenchyme cells moved, assume the apoptose if moved too far).

3.2.4 Model results: dynamics for larger tumor foci, immediate parenchyme apoptosis

Use the assumptions from larger tumors. (Poor flow in tumors, diffusion, parenchyme cells apoptose if near tumor cells).

4 Discussion and future directions Paul, Jessica, Shannon

Recap of what we've learned. Does it mesh well with curently known stuff? Does it help explain clinical stuff?

Future directions: critical to incorporate interstitial fluid flow with tumor cell volume changes. Likewise, need to drive porosity assumptions from tumor cell density. More direct, dynamical linking of codes.

Add biochemical signaling, active tissue remodeling (rather than just deformation), advective terms in BioFVM to replace the cylindrical far-field assumptions.

Follow-up. 3D is possible, but more insight on 3D lobular geometry, flow necessary. etc.

Acknowledgements PQ grant, BCRF grant, PSOC grant, support of CAMM, others?

5 Supplementary Materials Paul, Jessica

1. Digital cell lines for tumor cells, parenchyma
2. PhysiCell simulation source code

3. Simulation output data
4. Visualization routines
5. Analysis scripts
6. Anything else?

References

Gianluca D'Antonio, Paul Macklin, and Luigi Preziosi. An agent-based model for elasto-plastic mechanical interactions between cells, basement membrane and extracellular matrix. *Math. Biosci. Eng.*, 10(1):75–101, 2013. doi: 10.3934/mbe.2013.10.75. URL `http://dx.doi.org/10.3934/mbe.2013.10.75`.

Ahmadreza Ghaffarizadeh, Samuel H. Friedman, and Paul Macklin. Biofvm: an efficient, parallelized diffusive transport solver for 3-d biological simulations. *Bioinformatics*, 32 (8):1256–8, 2016. doi: 10.1093/bioinformatics/btv730. URL `http://dx.doi.org/10.1093/bioinformatics/btv730`.

Ahmadreza Ghaffarizadeh, Samuel H Friedman, Shannon M Mumenthaler, and Paul Macklin. Physicell: an open source physics-based cell simulator for 3-d multicellular systems. *PLoS Comput. Biol.*, 2016 (in review).

Kenichiro Nishii, Greg Reese, Emma C. Moran, and Jessica L. Sparks. Multiscale computational model of fluid flow and matrix deformation in decellularized liver. *Journal of the Mechanical Behavior of Biomedical Materials*, 57:201 – 214, 2016. ISSN 1751-6161. doi: http://dx.doi.org/10.1016/j.jmbbm.2015.11.033. URL `http://www.sciencedirect.com/science/article/pii/S1751616115004518`.

Kosuke Tsukada and Makoto Suematsu. Visualization and analysis of blood flow and oxygen consumption in hepatic microcirculation: Application to an acute hepatitis model. *J. Vis. Exp.*, 66:e3996, 2012. doi: 10.3791/3996. URL `http://dx.doi.org/10.3791/3996`.